nature structural & molecular biology

Reconstruction of the chemotaxis receptor–kinase assembly

Sang-Youn Park[1], Peter P Borbat[1,2], Gabriela Gonzalez-Bonet[1], Jaya Bhatnagar[1], Abiola M Pollard[1], Jack H Freed[1,2], Alexandrine M Bilwes[1] & Brian R Crane[1]

In bacterial chemotaxis, an assembly of transmembrane receptors, the CheA histidine kinase and the adaptor protein CheW processes environmental stimuli to regulate motility. The structure of a *Thermotoga maritima* receptor cytoplasmic domain defines CheA interaction regions and metal ion–coordinating charge centers that undergo chemical modification to tune receptor response. Dimeric CheA–CheW, defined by crystallography and pulsed ESR, positions two CheWs to form a cleft that is lined with residues important for receptor interactions and sized to clamp one receptor dimer. CheW residues involved in kinase activation map to interfaces that orient the CheW clamps. CheA regulatory domains associate in crystals through conserved hydrophobic surfaces. Such CheA self-contacts align the CheW receptor clamps for binding receptor tips. Linking layers of ternary complexes with close-packed receptors generates a lattice with reasonable component ratios, cooperative interactions among receptors and accessible sites for modification enzymes.

The signaling network that controls bacterial chemotaxis achieves remarkable sensitivity, gain, dynamic range and feedback control through the formation of two transmembrane protein complexes[1–4]. The first comprises an assembly of chemotaxis receptors (methyl-accepting chemotaxis proteins, or MCPs), the histidine kinase CheA, the receptor-coupling protein CheW, receptor-modification enzymes and localized phosphatases; the second embodies the multicomponent flagellar motor that propels and reorients the cell. The receptor complex interprets extracellular signals by tuning the activity of CheA, which in turn phosphorylates the response-regulator protein CheY. Phospho-CheY diffuses to the flagellar motor, binds the switch complex and affects the sense of flagellar rotation.

Most dimeric MCPs span the membrane with four helices (TM1, TM2, TM1′ and TM2′), bind ligands through an N-terminal periplasmic domain and bind cellular components through a C-terminal cytoplasmic domain[4], which is linked to TM2 by a short segment of unknown structure (the HAMP domain). The cytoplasmic domain of each MCP subunit folds as two long antiparallel helices that dimerize into a four-helix bundle[5]. The region most distal to the membrane (the tip of the bundle) interacts with CheA through the adaptor protein CheW[4]. At sites ~140–195 Å away from the receptor tip, specific glutamate residues undergo methylation (by CheR) and demethylation (by CheB or CheD) and specific glutamine residues undergo deamidation (by CheB or CheD) to tune receptor activation of CheA[4,6,7]. Regulation of the CheB methylesterase activity by CheA provides the system with feedback control (also known as adaptation). Changes in receptor conformation upon ligand binding probably involve a small (1–2 Å) piston motion of TM2 relative to TM1 (refs. 4,8). Understanding how such a movement, coupled with the influence of chemical modification, affects kinase activity rests on defining detailed interactions among CheA, CheW and receptors.

CheA consists of five separate functional units (P1 to P5), strung together as distinct domains over the length of the polypeptide[9]. P1 contains the substrate histidine autophosphorylated by the kinase domain (P4). P2 docks CheY for phosphotransfer from P1. The last three domains, P3, P4 and P5, comprise dimerization, kinase (ATP-binding) and receptor-coupling modules, respectively, and their structures have been determined together for the *T. maritima* enzyme (CheAΔ289)[10]. CheW has the same SH3 domain–like fold as the CheA P5 regulatory domain[10,11] and conserves two intertwined five-stranded β-barrels (designated subdomains 1 and 2 in CheW). The P3-proximal barrel of P5 binds the dimerization domain, whereas the P3-distal barrel symmetrically contacts another P5 domain in the crystal lattice of CheAΔ289 (ref. 10). The attachments of P1 and P2 to CheAΔ289 by long linker regions (typically 25–45 residues) increase the local concentrations of these modules in the vicinity of P3, P4 and P5 domains[12,13].

The clustering of MCPs at the poles of cells is dependent on CheW, somewhat dependent on CheA and, overall, essential for the signaling system to function[14–16]. Teams of receptors, with members of different receptor types, physically associate and influence one another's ability to transmit signals and undergo chemical modification[17–19]. A trimer of receptor dimers found in the crystal lattice of the Tsr cytoplasmic domain has been suggested as a key component of the signaling

[1]Department of Chemistry and Chemical Biology and [2]The Advanced ESR Technology Center, Cornell University, Ithaca, New York, 14853 USA. Correspondence should be addressed to B.R.C. (bc69@cornell.edu).

Received 17 January; accepted 13 March; published online 23 April 2006; doi:10.1038/nsmb1085

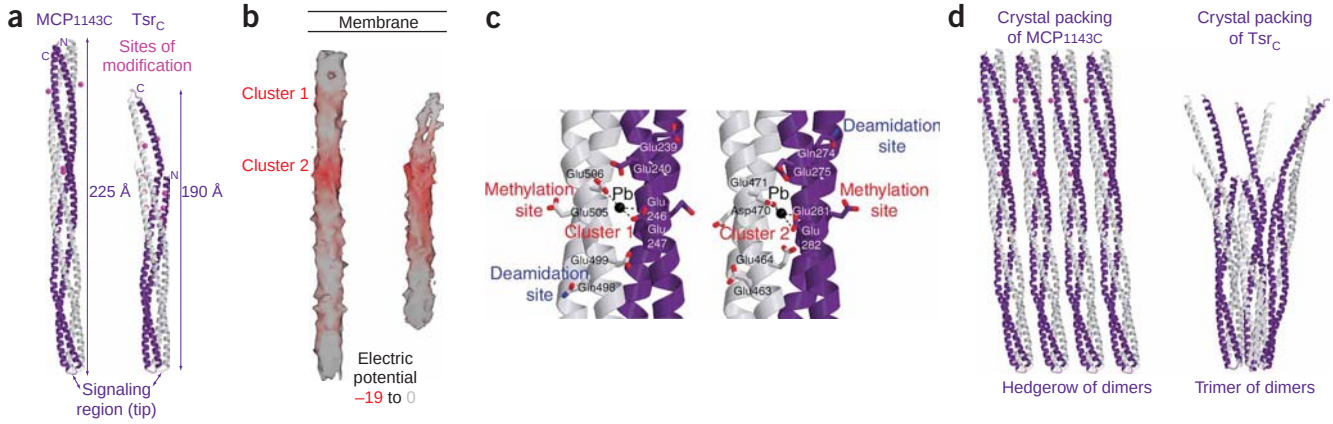

Figure 1 Structures of the cytoplasmic domains from *T. maritima* MCP_{1143C} and *E. coli* Tsr_C. (**a**) The MCP_{1143C} dimer (left, gray and blue subunits) is longer than Tsr (right) and has fewer, more separated methylation sites (magenta dots). Tsr_C may not fold as a complete bundle owing to N-terminal truncation[20]. (**b**) Solvent-accessible surface area of MCP_{1143C} (left) and Tsr_C (right) colored by electrostatic potential. Both receptors are completely negatively charged (red), with the highest potentials localizing at the modification sites. (**c**) The two metal-binding clusters of conserved residues in MCP_{1143C}. Seven carboxylates and one glutamine side chain surround the metal-binding sites in an arrangement that relates the two clusters with roughly two-fold symmetry. CheR and CheD target one glutamate residue and the glutamine residue of each cluster, respectively. The modification sites are accessible in the hedgerow. (**d**) Crystal packing of MCP_{1143C} compared to Tsr_C. Unlike Tsr_C, which packs as a trimer of dimers[20], MCP_{1143C} aligns as a hedgerow of dimers in one dimension; in the other dimension, layers of hedgerows stack staggered with respect to each other (not shown).

framework[20,21]. *In vivo* cross-linking experiments are consistent with such an arrangement in *Escherichia coli*, but do not preclude other assemblies[17]. Herein, we report crystallographic structures, pulsed-ESR solution studies and biochemical experiments on *T. maritima* chemotaxis proteins, which, when combined with previous data, allow reconstruction of possible core scaffolds for the signaling particle. The constraints imposed by these structures set boundaries for signaling mechanisms.

RESULTS

Structure of a *T. maritima* receptor signaling domain

The chemotaxis proteins of *T. maritima* share considerable homology with those of *E. coli*, but are better representatives for the chemotaxis systems of nonenteric bacteria. Compared to *E. coli* proteins, the *T. maritima* MCP receptors have unrelated periplasmic domains and longer cytoplasmic signaling regions. The 2.5-Å-resolution structure of the cytoplasmic domain (residues 225–530) of a *T. maritima* MCP receptor (locus tag tm1143; MCP_{1143} denotes the entire receptor and MCP_{1143C} the C-terminal cytoplasmic domain) was determined by MAD phasing of a tri-methyl lead acetate derivative (R_{free} = 28%; **Supplementary Fig. 1** online). The receptor fragment dimerizes to form a 225-Å-long four-helix bundle with a diameter of ~20 Å (**Fig. 1a**). Each subunit contributes two helices, CD1 and CD2, joined by a short, highly conserved U-turn at the bundle tip. CD1 immediately follows the ~30-residue HAMP domain, which directly attaches to TM2. The membrane-distal end of the MCP_{1143C} structure closely resembles that of the previously determined structure for the *E. coli* serine receptor cytoplasmic signaling domain, Tsr_C[20]. However, unlike the Tsr_C fragment crystallized, which lacks the first third of CD1 and thus appears as a partially unwound four-helix bundle, CD1 and CD2 tightly interact from start to end in MCP_{1143C} (**Fig. 1a**). Owing to contacts with another layer of staggered receptors within the lattice, the helical bundle kinks ~10°, 60 Å from the tip at Gly417, where a region of high residue conservation begins. Notably, similarly placed glycine residues at the boundary between the adaptation and signaling domains of the *E. coli* Tar receptor are important for signal transduction[22]. Relatively high *B*-factors of residues at the highly-conserved tip of MCP_{1143C} are consistent with this region gaining stability from CheA or CheW interactions.

Chemical modification sites

The structure of MCP_{1143C} includes modification sites targeted by the deamidase CheD and the methyltransferase CheR[6] (**Fig. 1a**,**b**). Acidic side chains that stripe down the superhelix of the bundle concentrate in three clusters that distribute at approximately eight-, six- and one-tenth of the length from the conserved tip (**Fig. 1a**,**b**). The two clusters closest to the point of membrane insertion (clusters 1 and 2) reside 60 Å apart on perpendicular faces of the receptor (**Fig. 1a**). Clusters 1 and 2 are pseudo two-fold symmetric to each other in their distribution of seven acidic side chains (glutamate and aspartate), one of which is targeted by the CheR methyltransferase and the CheD methylesterase *in vitro*[6] (**Fig. 1c**). CheD selectively deamidates an additional glutamine residue at the periphery of each cluster (**Fig. 1c**). One copy each of clusters 1 and 2 (note that there are four total per dimer) binds a lead ion in its center (**Fig. 1c**). In the copies that do not bind lead, direct hydrogen bonds link the glutamate residues that would otherwise coordinate metal ions. Isothermal titration calorimetry experiments combined with site-directed mutagenesis studies reveal that cluster 2 binds Zn^{2+}, but not Ca^{2+} or Mg^{2+}, with moderate affinity (dissociation constant of 1.1 μM). The high negative charge of clustered signaling domains proximal to the membrane (**Fig. 1b**) may enhance stabilizing interactions with cations. Changes of modification state in these clusters will also influence receptor net charge and metal-binding properties. Mutations of similarly clustered glutamate residues in *E. coli* Tar produce a 'super-activated' state[23].

Receptor self-associations

In the crystal, the *E. coli* Tsr fragments interact via their conserved tips to form a trimer of dimers (**Fig. 1d**) that has been implicated as the cooperative unit for receptor signaling[2,3,20]. Even though MCP_{1143C} conserves most of the Tsr tip residues involved in the trimer contact, MCP_{1143C} does not form a trimer of dimers in the crystal. Instead, the

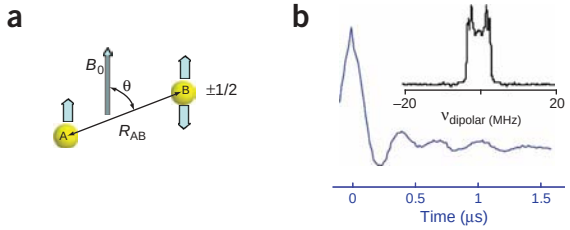

c

Intradomain and selected interdomain distances (Å)

Mutated site	Ser15	Ser72	Ser80	Asn553	Ser568	Asp579	Glu646
Ser15		27 & 29[a]	18.2	37	54.5	61	43.7
Ser72	X		24.5 & 30[a]	27	49	46	32.5
Ser80	X	X		26	47	54.5	39.5
Asn553	X	X	X		23.5	34.5	32
Ser568	X	X	X	X		32.5	35.5
Asp579	X	X	X	X	X		28
Glu646	X	X	X	X	X	X	

[a]Second (minor) conformation with better-defined position.

Figure 2 Pulsed ESR for reconstructing protein-protein complexes. (**a**) Electron spins of two nitroxides, separated by R_{AB}, are coupled by the dipole-dipole interaction $a = \gamma_e^2(1 - 3\cos^2\theta)/r^3$, where θ is the angle between the direction of magnetic field B_0 and R_{AB}, $r \equiv |R_{AB}|$, γ_e is the gyromagnetic ratio for the electron. (**b**) DQC signal for the CheA dimer labeled at residue 318, plotted against the relevant time variable ($t_m - 2t_p$). Here, t_p is the time between the first pulse (π/2) and the second pulse (π) and also between the second pulse and the third pulse (π/2) of the six-pulse DQC sequence[47]; $2t_m$ is the time between the first pulse and the spin echo. t_p is stepped out with $2t_m$ fixed. The Fourier-transformed signal (inset) gives rise to the dipolar spectrum, from which coupling, *a*, and hence distances are inferred. (**c**) Distances between spin labels on CheW (Ser15, Ser72, Ser80) and CheA P5 (Asn553, Ser568, Asp579, Glu646) derived from pulsed ESR.

receptors align as a hedgerow of dimers (**Fig. 1d**) in which the dimer-to-dimer contact buries much more surface area between receptors (1,873 Å^2 per dimer) than that in the trimerization interface of *E. coli* Tsr (788 Å^2 per dimer). In the aligned hedgerow, cluster 1 lies directly within the interdimer contact, with some conserved glutamate residues (for example, Glu499) hydrogen-bonding with a symmetry-related residue on the adjacent dimer. Neighboring receptors in the lattice surround cluster 2 but do not interface as closely with these residues. The third, tip-proximal cluster does not bind lead ions in the lattice, but it also supplies contacts between receptors in the hedgerow, including symmetric glutamate-to-glutamate hydrogen-bonding across aligned dimers (Glu429 and Glu436). The contacts that align the MCP_{1143C} domains in the crystal allow access to all of the modification sites from the side.

ChеW–CheA complex mapped by pulsed ESR

To map the interaction between CheA domain P5 and CheW, site-specific spin-labeling was combined with pulsed-ESR techniques to measure intermolecular distances between sites in the CheA–CheW complex of *T. maritima* (**Figs. 2** and **3**). This represents the first time that pulsed ESR, which has the ability to define long interspin distances (10–80 Å), has been applied to determine the mode of interaction between two proteins. On the basis of the crystal structure of CheAΔ289 (ref. 10) and the NMR structure of CheW[11], four sites in P5 (Asn553, Ser568, Asp579 and Glu646) and three sites in CheW (Ser15, Ser72 and Ser80) were mutated to cysteine and labeled with a nitroxide spin label (MTSSL). Twelve distances between pairs of spin labels were extracted from dipolar couplings to give CheW-to-P5 distances. Distance geometry followed by rigid-body refinement against the distance restraints produced a clash-free complex of the CheAΔ289 crystallographic structure[10] and the CheW NMR structure[11]. The resulting model places the end of CheW subdomain-2 (residues 40–60) adjacent to the end of the P5 proximal barrel (residues 635–660; subdomain-1) (**Fig. 3a**,**b**). The surface of CheW buried in the CheA interaction agrees well with the results of mutations that disrupt the CheA-CheW interface[24–26] and with changes in NMR signals upon complex formation[11,27].

The structure of CheA P4-P5 bound to CheW

The validity of the ESR-derived complex was confirmed by the 3.5-Å-resolution crystal structure of CheAΔ354 (domains P4 and P5) bound to CheW in the presence of ADPNP (a nonhydrolyzable analog of ATP). This crystal structure comprises two CheAΔ354 and two CheW per asymmetric unit (R_{free} = 29%; **Supplementary Fig. 2** online). A tight interaction between the P5 proximal barrel and CheW subdomain-2 buries ~1,050 Å^2 of surface area per domain and includes conserved hydrophobic residues at each barrel's end that are found throughout the CheW-P5 family (**Fig. 3b**).

The two P4-P5–CheW molecules in the asymmetric unit have different orientations of P4 relative to P5 (**Fig. 3c**). In conformation A, P4 rotates nearly 90° about the link between P4 and P5 to bind a surface of P5 where P3 would normally be docked in the CheA dimer (**Supplementary Fig. 3** online). In conformation B, P4 and P5 have the same orientation as they do in the CheAΔ289 crystal structure, although P4 has weak electron density at its periphery owing to lack of contacts with other molecules in the lattice.

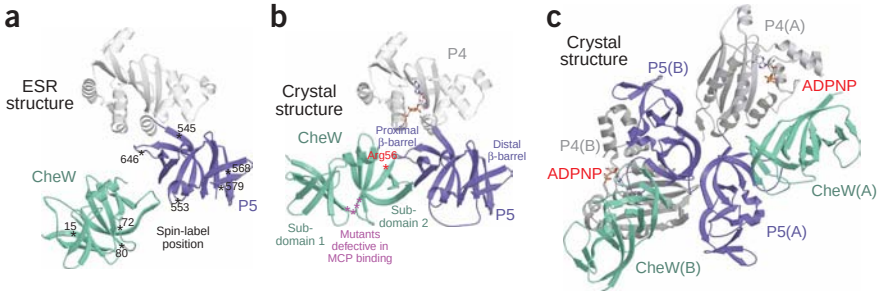

Figure 3 CheW-CheA interactions. (**a**) CheW-P5 interaction determined by the pulsed-ESR experiment. Distances between spin labels (black asterisks) predict that CheW subdomain-2 (shown as NMR solution structure) binds the P5 proximal β-barrel (from CheAΔ289 crystal structure). (**b**) Crystal structure of the CheAΔ354–CheW B conformation with secondary structure showing the topological equivalence of P5 and CheW. The proximal β-barrel of P5 (subdomain-1) binds subdomain-2 of CheW. Residues essential for linking the CheA–CheW complex to MCP receptors in *E. coli* reside on the loop connecting the two P5 β-barrels (magenta asterisks)[24,31]. (**c**) The crystal structure of CheW bound to CheA domains P4 and P5. Two molecules of CheAΔ354–CheW in the asymmetric unit (conformations A and B) have different orientations of P4 (gray ribbons, with ADPNP shown in stick representation) relative to P5 (blue ribbons), although CheW (green ribbons) binds P5 the same way for both complexes.

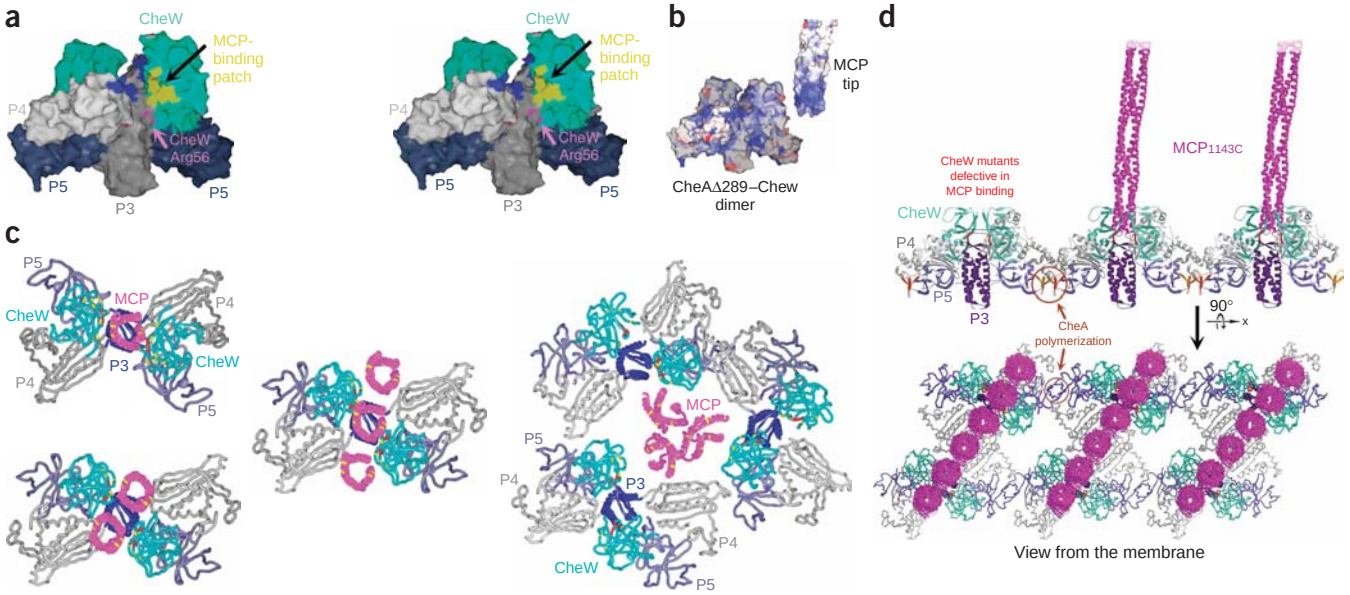

Figure 4 Structural implications for the CheA–CheW–MCP_{1143C} complex. (**a**) Regions where receptors interact with the CheA–CheW complex (stereographic view). Residues defined from genetic suppressor screens[29] or biochemical binding assays[24,31] as important for receptor interactions (yellow surface; residues 27, 30, 32, 33, 80, 81, 98, 101) map onto the solvent-accessible surface of the cleft formed by the two CheW proteins (green) in their complex with CheA (medium gray, P3; light gray, P4; dark gray, P5). Highly conserved positive residues (blue; residues 297, 364, 367, 378) on P3 and P4 face the same cleft. Arg56 (magenta), a CheW residue key for kinase regulation by the receptor, interacts with the P3 dimerization domain, as do conserved acidic residues (red, residues 390, 397, 401) on P4. (**b**) Residue conservation mapped onto the surface of CheA–CheW and MCP_{1143C}. Highly conserved regions (dark blue, most conserved; dark red, least conserved) localize in the cleft formed by CheW and at the tip of the receptor. Seventeen representative CheA–CheW sequences and 50 MCP sequences provided the conservation scores as defined by CONSURF[53]. (**c**) Possible symmetric interactions between receptors and CheW (viewed from the membrane). Suppressor mutation sites (yellow tubes) on the receptor (*T. maritima* residues 359, 360, 387, 398) or CheW (residues 56, 80, 98, 101) rescue defects in the binding partner[29]. Mutations at CheW positions 12 (also yellow), 30, 56, 96 and 101 generate proteins that suppress chemotaxis in the presence of wild-type CheW (dominance)[29]. CheW-site mutants (residues 27, 30, 32, 33, 35; red tubes) also diminish receptor binding *in vitro*[24,31]. Receptors are shown associated by contacts found in the MCP_{1143C} crystal. For the binding of a single receptor, the P5–CheW–P4 assembly was rotated slightly about the P3 hinge to allow full contact between the receptor and the functionally defined residues. Right, three CheA–CheW dimers associated around one trimer of MCP_{1143C} dimers modeled on the crystallographic assembly of Tsr_C[20] cannot engage all of the receptor-binding residues in the CheW cleft simultaneously or satisfy P5-P5 interactions. (**d**) CheW–CheAΔ289–receptor complex. Top, two CheW molecules (green) positioned on the CheAΔ289 dimer form a clamp at the top of the P3 dimerization domain (indigo). Forty ESR distance measurements between positions (some denoted with dotted lines) confirm the CheW and CheA domain positions in the complex. Mutations resulting in defective MCP binding map to surface-exposed residues deep in the clamp (red)[24,31]. Association of CheA through P5-P5 self-interactions found in two crystal structures aligns the CheW clamps. The tip of MCP_{1143C} (magenta) fits into the CheW clamp, making contact with the receptor-binding residues identified by mutagenesis studies. Bottom, an assembly of ternary complexes linked through P5-P5 contacts and closed-packed receptor interactions, as defined in the MCP_{1143C} crystals. Holes in the lattice allow access for the modification enzymes and possibly higher receptor ratios under some conditions.

A dimeric CheAΔ289–CheW complex

A similar spin-labeling strategy was applied to determine domain orientations in solution complexes of dimeric CheAΔ289 with CheW (**Table 1**). To verify the position of P3 relative to P5, we generated CheA heterodimers in which P3 residue 318 and P5 residue 545 were labeled only in the same subunit or one set of 318 and 545 spin labels were held by opposite subunits. The ESR-measured intrasubunit and intersubunit distances between residues 318 and 545 (14 and 30 Å, respectively) agree well with those separations predicted by the P3-P5 domain juxtapositions in the CheAΔ289 dimer (12 and 30 Å, respectively). Furthermore, distances from intersubunit, symmetric labels indicate that the positions of P3, P4 and P5 were largely unchanged by the addition of unlabeled CheW, with exceptions of 3- to 8-Å changes in distances between residues 387 (P4 to P4′), 545 and 568 (both P5 to P5′) (**Fig. 4a** and **Table 1**).

To verify simultaneous binding of two CheW molecules to one CheAΔ289 dimer, we determined that inter-CheW distances between spin labels at sites 15, 72, 80 and 139 in the presence of wild-type CheAΔ289 (60, 67–70, 59–60 and 50 ± (10–15) Å, respectively) correlated well with distances between Cα atoms in our reconstructed CheW–CheAΔ289 complex (47, 73, 51 and 43 Å, respectively). These results further confirm that the CheW molecules reside at the top of the CheAΔ289 dimer in close proximity to each other (**Fig. 4a**). The intersubunit CheA distances between labels at residues 387 (P4 to P4′), 318 (P3 to P3′) and 545 or 646 (P5 to P5′) in the presence and absence of CheW also support a solution structure of the CheW–CheAΔ289 complex that maintains P3-P4-P5 domain orientations related to those found in the CheAΔ289 crystal. The measured distances between labels on CheW (residue 80) and domain P3 (residue 318) or P4 (residues 387, 496 and 508), which were 43, ≥40, ≥25 and ≥40 Å, respectively (**Table 1**), also agree with the crystal structure.

Interactions between CheW and P3

The solution structure of CheAΔ289 and CheW predicts an interaction of CheW with P3. Accordingly, the affinity of CheW for CheA increases when P3 is fused to P4-P5 (K_d = 10 versus 135 nM) and actually decreases for P4-P5 relative to P5 alone (36 nM). A P3-CheW

Table 1 Interdomain distances in the CheAΔ289–CheW complex (Å)

Domains	Residue pair[a]	Proteins in sample	Model D (Å)	ESR D average (Å)	ESR range[b] (Å)
P4-P4	A387-B387	CheA	42	44	30%
	A387-B387	CheA + CheW	42	46	30%
	A496-B496	CheA	90	65	30%
	A496-B496	CheA + CheW	90	N/A	N/A
P3-P3	A318-B318	CheA	22	28	26 & 30
	A318-B318	CheA + CheW	22	28	26 & 30
P3-W	318-W80	CheA + CheW	35/44	43	30%
P4-W	387-W80	CheA + CheW	16/43	40–50	
	387-W15	CheA + CheW	17/44	40–50	
	387-W72	CheA + CheW	28/50	40–50	
P4-P5	508-646	CheA + CheW	15/65	25	22–38
P5-P5	A568-B568	CheA	76	49	30%
	A568-B568	CheA + CheW	76	57	30%
	A545-B545	CheA	40	41	35–50
	A545-B545	CheA + CheW	40	38 ± 1	32–50
	A646-B646	CheA	62	N/A	N/A
	A646-B646	CheA + CheW	62	61	30%
	A553-B553	CheA	63	64	30%
	A553-B553	CheA + CheW	63	N/A	N/A
W-W	W15-W15	CheA + CheW	49	60	30%
	W80-W80	CheA + CheW	51	59–60	30%
	W72-W72	CheA + CheW	70	67–70	30%
	W139-W139	CheA + CheW	43	50	
P5-P3	A545-A318	CheAHD[c]	12	14	Tail up to 30
	A545-A318	CheAHD + CheW	12	14	Tail up to 30
	A545-B318	CheAHD	30	30	Tail up to 45

[a]A, CheA monomer A; B, CheA monomer B; W, CheW. [b]Signal shapes reflected distributions in distances that were confined within ±15% in the most cases. [c]CheA heterodimer.

contact also explains why CheW decreases the rate of CheA dimer exchange[28] and agrees with a 43-Å ESR distance between P3 residue 318 and CheW residue 80 (**Table 1**). In the CheW–CheAΔ289 complex, the tip of CheW loop β4-β5 juxtaposes invariant residue Arg56 with conserved P3 residue Asp345. Mutation of the Arg56 equivalent in *E. coli* CheW (for example, R62H) has only minor effects on kinase binding, activation and receptor association, but completely disrupts chemotaxis *in vivo*[24] and has the ability to suppress the effects of defective MCPs[29]. Thus, interactions between CheW and P3 may be important in signaling. Because CheW interacts with P5, the P3-CheW contact also stabilizes the interface between P3 and P5, which is key for positioning the two CheW molecules above the P3 domain.

The P4 kinase domain

In crystal structures of both the CheAΔ289 dimer and the CheAΔ354–CheW complex, conformation B, P4 is in the same position relative to P3 and P5. However, dipolar couplings between spin labels on P4 at two different positions (387 and 508) and labeled P3 (residue 318) or P5 (residue 545) in the CheAΔ289–CheW complex gave only broad signals (**Table 1**). Thus, P4 samples a wide range of orientations in solution, consistent with the few contacts between P4 and either P3 or P5 in the CheAΔ289 crystal structure. Furthermore, the lack of change in P4 flexibility in the absence of CheW rules against strong binding between P4 and CheW. In full-length *T. maritima* CheA, the substrate-containing P1 domain also seems to sample a very broad distribution of positions, as no fixed distances were observed by ESR between spin-labeled sites on P1 and domains P3-P5 (data not shown).

P5-P5 contacts mediate CheA self-association

Extensive symmetric interactions between two P5 domains, via an exposed surface that conserves its hydrophobic nature across CheA sequences, associate CheA molecules in both the CheAΔ354–CheW and CheAΔ289 crystals (840 $Å^2$ buried surface per P5). Site-directed mutants in P5 subdomain-2, near or at the surface that mediates P5-P5 contacts, reduce the ability of attractant to deactivate CheA *in vivo*[30].

Receptor-kinase interactions

The reconstructed CheW–CheAΔ289 complex places the two CheW molecules facing each other and forming the walls of a ~22-Å-wide canyon, the bottom of which is made by the two short strands capping the P3 dimerization domain (**Fig. 4**). The segments in CheW flanking the edge of the canyon include the loop connecting the two β-barrels (residues 26–33). A mutant screen for loss of binding between *E. coli* CheW and the Tar MCP has identified four key positions in this CheW loop that also affect receptor binding *in vitro*[24,31]. A separate study has shown that *E. coli* CheW suppressor mutants rescue chemotaxis in cells containing compromised Tsr MCPs[29]. These allele-specific suppressor mutations localize to the same CheW face that contains the loss-of-binding mutations mentioned above, and hence they potentially represent points of contact with the receptors (**Fig. 4a**). In addition, highly conserved positively charged residues on the CheA P4 domain (*T. maritima* CheA residues Arg364, Arg367 and Arg370) face the cleft formed by the two CheW proteins (**Fig. 4b**). With one receptor dimer aligned directly above the P3 domain, the conserved tip fits well into the cleft generated by the two CheW proteins (**Fig. 4c**). Alternatively, the receptor bundle's axis could be offset from the P3 domain's two-fold axis and still allow the receptor tip to contact the binding patch on CheW from the side (**Fig. 4c**). Offsetting the receptor tip in a direction that projects it over the P4 domains allows two receptors to simultaneously bind, one to each CheW; for full contact with the binding patch on CheW, the two receptor dimers must essentially close-pack, as they do in the MCP_{1143C} crystal lattice. Three interacting receptor dimers could also be engaged by one dimeric CheW–CheA if the CheW proteins bound at the interface between receptors (**Fig. 4c**). Notably, a trimer of MCP dimers would be too large to be accommodated above the P3 domain in the cleft between the two CheW proteins (**Fig. 4c**). Alternatively, one unit of the Tsr trimer of dimers could contact only one CheW receptor-binding patch on the side. However, two additional CheA–CheW dimers could not then approach close enough to engage the other two symmetric surfaces of the trimer without substantial steric collisions or considerable rotation of the P5-CheW unit away from P3 (**Fig. 4c**). Clustering CheA dimers around the Tsr trimer would also prevent P5-P5 self-interactions.

DISCUSSION

Positioning of one receptor dimer on top of P3, with two additional receptor dimers interacting to the side, produces a stoichiometry of

three receptor dimers to one CheA dimer to two CheWs (**Fig. 4c**). Although estimates of the MCP–CheA–CheW stoichiometries vary greatly *in vivo* and *in vitro*[32–37], this assembly does agree with recent ratios deduced from the cellular stoichiometry of *E. coli* chemotaxis proteins[34] and Hill analysis on the *E. coli* Tar[36] and unmodified Tsr receptors[35]. For Tsr[35], but not Tar[36], cooperativity increases dramatically with glutamate methylation. Such behavior could derive from receptor self-interactions driven by charge neutralization, as we observed in the low-pH MCP_{1143C} crystals. Close association of receptor tips in *E. coli* is also supported by the results of Tsr mutations at the contact sites in the crystallographic trimer, which can influence the functions of other receptors[18]. EM reconstructions (21-Å resolution) of active ternary complexes assembled by leucine-zipper substitution of TM1 and TM2 show a receptor alignment similar to that in the MCP_{1143C} crystal lattice, but also reveal bilateral symmetry to the particle, which is difficult to reconcile with membrane association[37,38].

An extended lattice of receptors and kinases has been suggested as a means to quantitatively explain gain and cooperativity in chemotaxis[3,39,40]. Different receptor types closely associate in *E. coli*, and CheA and CheW inhibit exchange of new receptors into these clusters[41]. An extended lattice can be generated by the interactions defined by the *T. maritima* proteins. However, the CheA-CheW contacts proposed in previous lattice models[39] are inconsistent with our experimentally determined structures. Assembling successive CheA molecules through the P5-P5 contact aligns the CheW receptor-binding patches and thereby satisfies the spatial constraint that results from receptors projecting their tips a fixed distance from the membrane (**Fig. 4c**). With the interaction surfaces of the CheA P5 domain occupied by self-association and binding to CheW, receptor-to-receptor contacts probably link layers of ternary complexes. One such assembly, modeled on the basis of the MCP_{1143C} crystal contacts, produces an MCP dimer/CheA dimer/CheW ratio of 3:1:2, provides symmetric interactions between the CheW patches and allows room for adaptation enzymes to access the modification sites (**Fig. 4d** and **Supplementary Fig. 4** online). With the P3 and MCP_{1143C} bundle axes coincident, the P4 domains are below the receptor tips, with the ATP-binding sites directed up toward the membrane, below the position from where the CheA P1 domain would project. Structures of the MCP_{1143} periplasmic ligand-binding domains are unknown; however, flexibility in structurally undefined regions separating MCP_{1143C} from the periplasmic region could allow for many possible arrangements of the ligand-binding domains that would maintain interactions among the cytoplasmic signaling regions.

The *T. maritima* crystal and ESR structures are difficult to reconcile with a continuous lattice based on a trimer-of-dimers receptor topography, as found in the structure of Tsr_C (**Fig. 4c**). Cross-linking of cysteine-modified receptors in *E. coli* by trivalent agents does support a trimer-of-dimers receptor assembly[17]. However, the observation that substitution of a bulky tryptophan at the trimer interface does not alter the cross-linking pattern leaves open some questions regarding the exact structure of the interacting *E. coli* receptors[17]. Nevertheless, receptor organization in all bacteria may not be the same. Notably, a phenylalanine residue (373) that stabilizes the Tsr trimer interface by forming a symmetric hydrophobic cluster is replaced by a glutamate in all of the *T. maritima* transmembrane MCPs.

To process signals, the receptor array probably controls the accessibility of CheA P1 for P4 in response to changes in receptor conformation or clustering. Notably, a complex formed *in vitro* from one receptor dimer, one CheA dimer and two CheW proteins inhibits the *E. coli* kinase, whereas higher receptor stoichiometries activate it[35,37,42]. Small movements of the CheW-P5 unit about P3 may allow repositioning of the receptor-binding patch and switching among different receptor interactions (**Fig. 4c**). At the pivot point for this movement lies Arg56, the residue whose mutation disables kinase regulation without affecting receptor binding (**Fig. 4a**). Engaging the conserved positive residues of P4 with the negatively charged receptor tips would block binding of P1. Receptor-receptor interfaces that involve the modification sites would be effective at communicating conformational changes among the receptors. To maintain symmetric contacts, changes in the conformation of one receptor would be relayed to an interacting partner. The full spectrum of signaling may well involve transitions between different association modes and even restructuring of the array[16,35]. Nevertheless, our structural work suggests that the signaling architectures incorporate one CheA dimer and two CheW molecules to form a symmetric binding patch for receptor tips either directly above or above and adjacent to the CheA P3 domain.

METHODS

Protein preparation. Genes encoding the cytoplasmic domain (residues 225–530) of *T. maritima* MCP_{1143C}, CheAΔ289 (P3-P4-P5 domain, 290–671), CheAΔ354 (P4-P5 domain, 355–671), CheAΔ539 (P5 domain, 540–671) and CheW (1–151) were PCR-cloned into the vector pET28a (Novagen), and the corresponding proteins were expressed with an N-terminal His_6 tag and purified as described previously[10]. For CheA–CheW complex formation, the two concentrated proteins were mixed at a ~1–3 molar ratio of dimeric CheA–CheW and purified on a Superdex75 26/60 column in gel-filtration buffer (100 mM Tris (pH 7.5), 150 mM NaCl). All point mutations were introduced by QuikChange mutagenesis (Stratagene).

Crystallization and data collection. MCP_{1143C} crystals grew as needle clusters after 3 months from a 2-μl drop (1:1 mixture of 25 mg ml^{-1} protein in gel-filtration buffer and reservoir) by vapor diffusion against a reservoir of 2.2–2.6 M 1,6-hexanediol, 0.1 M sodium acetate (pH 4.5) and 2%–5% (v/v) of either ethanol or isopropanol. Diffraction data for both native, lead-derivatized (grown with 1 mM tri-methyl lead acetate) and selenomethionine (SeMet)-substituted MCP_{1143C} crystals (space group $P2_1$; one dimer per asymmetric unit; 33% solvent) were collected at 100 K by centering the synchrotron beam on an extended single-crystal fragment. All diffraction data (2.5- to 3.5-Å resolution; **Table 2**) were processed by the HKL package[43].

Crystals of CheAΔ354–CheW grew after 1 d from a ~2-μl drop (1:1 mixture of 50 mg ml^{-1} protein and reservoir) by vapor diffusion against a reservoir of 3%–5% (w/v) PEG 4000 with 0.1 M sodium acetate (pH 4.5), 1 mM tri-methyl lead acetate and 1 mM ADPNP. The crystals (space group $P4_12_12$; two copies of CheAΔ354–CheW per asymmetric unit; 72% solvent) diffracted to 3.5-Å resolution at 100 K after brief soaking in reservoir containing 40% (v/v) ethylene glycol.

Structure determination and refinement. Anomalous scattering from lead-derivatized MCP_{1143C} and SeMet-substituted protein were used for experimental phase determination. The model was built manually into solvent-flattened electron density maps, making use of selenium sites to set the sequence. The final 2.5-Å-resolution model (MCP_{1143C} residues 225–530) was then refined with CNS[44] to *R*-factor = 0.232 and R_{free} = 0.279 for $F > 2\sigma(F)$.

Initial phases for CheA–CheW were derived from a molecular-replacement solution of one *T. maritima* P4 domain and one P5 domain (PDB code 1B3Q). Two additional CheA domains and two CheWs were placed manually in the map and iteratively refined with CNS to *R*-factor = 0.250 and R_{free} = 0.289 at 3.5-Å resolution (**Table 2** and **Supplementary Methods** online).

Isothermal titration calorimetry. Calorimetric measurements were carried out using a VP-ITC titration calorimeter (MicroCal) at 26 °C and data was extracted with the Origin software package. Native and mutant MCP_{1143C} were treated with thrombin for ~2–3 d to completely remove the His tag and

Table 2 Data collection, phasing and refinement statistics

	MCP_{1143C}	Lead #1			Lead #2		SeMet	CheAΔ354–CheW
Data collection								
Space group	$P2_1$	$P2_1$			$P2_1$		$P2_1$	$P4_12_12$
Cell dimensions								
a, *b*, *c* (Å)	24.6, 99.1, 117.2	24.6, 99.4, 117.2			24.7, 98.9, 117.5		24.6, 99.1, 117.2	136.6, 136.6, 231.3
α, β, γ (°)	90, 90.1, 90	90, 90.5, 90			90, 90.1, 90		90, 90.1, 90	90, 90, 90
		Peak	*Inflection*	*Remote*	*Inflection*	*Remote*	*Peak*	
Wavelength	0.98	0.9498	0.9506	0.9184	0.9497	0.9184	0.9790	1.1
Resolution (Å)	30–2.6 (2.64–2.6)	30–2.5 (2.59–2.5)	30–2.7 (2.8–2.7)	30–2.7 (2.8–2.7)	30–2.7 (2.8–2.7)	30–2.7 (2.8–2.7)	50–3.5 (3.63–3.5)	30–3.5 (3.63–3.5)
R_{sym}	0.119 (0.43)	0.098 (0.49)	0.093 (0.41)	0.110 (0.50)	0.110 (0.33)	0.107 (0.27)	0.142 (0.27)	0.09 (0.58)
$I / \sigma I$	14 (3)	21 (3)	17 (3)	11 (2)	17 (3)	16 (3)	10 (5)	40 (10)
Completeness (%)	98.1 (94.3)	99.6 (98.4)	99.1 (96.3)	98.6 (93.7)	98.1 (83.6)	96.3 (64.5)	86.0 (70.5)	99.8 (100)
Redundancy	3.5	7.0	3.4	3.4	3.5	3.5	3.0	15.0
Refinement								
Resolution (Å)		2.5 (2.6–2.5)						3.5 (3.6–3.5)
No. reflections		29,602						27,869
R_{work} / R_{free}		0.24/0.28 (0.33/0.38)						0.25/0.29 (0.26/0.30)
No. atoms								
Protein		4,630						7,058
Ligand/ion		2						62
Water		585						14
B-factors								
Protein		58						117
Ligand/ion		78						190
Water		59						77
R.m.s. deviations								
Bond lengths (Å)		0.009						0.009
Bond angles (°)		1.3						1.6

One crystal used for each dataset. Highest-resolution shell is shown in parentheses.

prevent its interference with metal-binding studies. The proteins were dialyzed overnight in gel-filtration buffer with 25 mM EDTA to remove trace metals. EDTA was back-dialyzed from the proteins in four separate steps (1/1,000 volume each time) using gel-filtration buffer pretreated with Chelex 100 (BioRad). The elimination of His tags from the samples was checked by MALDI MS. $MgCl_2$, $CaCl_2$ and $ZnCl_2$ solutions (7–10 mM) were prepared with the Chelex 100–treated gel-filtration buffer. Protein concentrations were determined by RC/DC assay (BioRad) with cytochrome c standards (MCP_{1143C}, 66.0 kDa; CheAΔ289, 42.7 kDa; CheAΔ354, 35.0 kDa; CheAΔ539, 14.6 kDa; CheW, 17.0 kDa). Corrections to the observed binding constants due to chelation of Zn^{2+} by Tris base were determined to be minor (less than 10% of observed K_d) owing to the weak affinity of Tris base for Zn^{2+} ($K_d \sim 10^2$) and the relative concentrations of competing species employed in the titrations.

Protein mutagenesis and spin-labeling. Four residues in the P5 domain of CheAΔ289 (Asn553, Asp579, Ser568 and Glu646) and three residues in CheW (Ser15, Ser72 and Ser80) were separately mutated to cysteines. Neither protein contains cysteines in its native sequence. In addition, all possible double mutations in CheAΔ289 and CheW were generated for measuring intrasubunit distances within each protein. Proteins were labeled for 4 h at 4 °C with 5–10 mM 1-oxyl-2,2,5,5-tetramethylpyrolinyl-3-methyl)-methanethiosulfonate (MTSSL; Toronto Research, Toronto) in gel-filtration buffer while the His-tagged proteins were bound to nickel–nitrilotriacetic acid agarose beads. The proteins were eluted after 6–12 h in the presence of thrombin. To establish interdomain separations, several other cysteine mutants (S318C, Q545C, E387C, K496C, D508C, S318C Q545C, E387C Q545C, D508C D579C, D508C E646C and CheW D139C) were generated and spin-labeled.

Pulse-ESR measurements. To measure distances, we applied two pulse-ESR techniques: six-pulse double quantum coherence (DQC)[45–47] and four-pulse double electron-electron resonance (DEER)[48,49] at 17.5 GHz on a specially constructed 2D-FT ESR spectrometer (**Supplementary Methods**)[50]. DEER provided satisfactory signal-to-noise ratios (SNR) for higher concentrations, reduced problems with deuterium modulation and had less signal attenuation in the presence of more than two spins compared to DQC. However, for cases of short distance or low spin concentration, DQC improves the SNR by a factor of 2–3. Comparisons between DQC and DEER were used to confirm the results. Signal recording at 60–70 K on samples (15–150 μM in 15–20 μl) usually took less than 30 min, but in a few cases where long distances (50–65 Å) were of interest, 2–12 h were necessary. Perdeuterated solvents (D_2O and 30% (w/v) glycerol-d8) increased phase relaxation times for nitroxides. The longer signal evolution (that is, larger t_m; see **Fig. 2**) enhanced resolution and access to longer distances. The average distance between nitroxide labels was estimated by Fourier-transforming the time-domain experimental data to obtain the singular frequencies of the Pake pattern function[51] (**Fig. 2b**) or by evaluating the half-width of a bell-shaped dipolar spectrum or the duration for the signal to decay 50% in the time domain. In cases of highly heterogeneous spin separations, average distances and distributions were obtained through direct inversion by Tikhonov regularization[52].

CheAΔ289 S318C Q545C and CheAΔ289 wild-type heterodimer. Equimolar amounts of CheAΔ289 S318C Q545C dimer with the His tag removed and CheAΔ289 wild-type dimer with the His tag intact were mixed at 65 °C for 10 min to enable subunit exchange[28]. His-tagged heterodimers and remaining wild-type homodimers were purified from dimers without His tags by nickel–nitrilotriacetic acid affinity chromatography at 4 °C, to minimize further subunit exchange, and then reacted with MTSSL.

Accession codes. Protein Data Bank: Coordinates have been deposited with accession codes 2CH7 (MCP_{1143C}) and 2CH4 (CheAΔ354–CheW).

Note: Supplementary information is available on the Nature Structural & Molecular Biology website.

ACKNOWLEDGMENTS

We thank C. Arango for help with distance-geometry calculations, C. Kim for advice on crystal growth, S. Oga and W. Hubbell for advice on nitroxide spin-labeling, J.S. Parkinson, R. Alexander, I.B. Zhulin and J.J. Falke for helpful discussions and NSLS, CHESS and NE-CAT at the Advanced Photon Source for access to data-collection facilities. This work was supported by US National Institutes of Health grants GM:R01066775 (to B.R.C.) and NCRR:P41-RR016292 (to J.H.F.).

COMPETING INTERESTS STATEMENT

The authors declare that they have no competing financial interests.

Published online at http://www.nature.com/nsmb/
Reprints and permissions information is available online at http://npg.nature.com/reprintsandpermissions/

1. Wadhams, G.H. & Armitage, J.P. Making sense of it all: bacterial chemotaxis. *Nat. Rev. Mol. Cell Biol.* **5**, 1024–1037 (2004).
2. Parkinson, J.S., Ames, P. & Studdert, C.A. Collaborative signaling by bacterial chemoreceptors. *Curr. Opin. Microbiol.* **8**, 116–121 (2005).
3. Sourjik, V. Receptor clustering and signal processing in *E. coli* chemotaxis. *Trends Microbiol.* **12**, 569–576 (2004).
4. Falke, J.J. & Hazelbauer, G.L. Transmembrane signaling in bacterial chemoreceptors. *Trends Biochem. Sci.* **26**, 257–265 (2001).
5. Falke, J.J. & Kim, S-H. Structure of a conserved receptor domain that regulates kinase activity: the cytoplasmic domain of bacterial taxis receptors. *Curr. Opin. Struct. Biol.* **10**, 462–469 (2000).
6. Chao, X. *et al.* A receptor-modifying deamidase in complex with a signaling phosphatase reveals reciprocal regulation. *Cell* **124**, 561–571 (2006).
7. Szurmant, H. & Ordal, G.W. Diversity in chemotaxis mechanisms among the bacteria and archaea. *Microbiol. Mol. Biol. Rev.* **68**, 301–319 (2004).
8. Ottemann, K.M., Xiao, W., Shin, Y-K. & Koshland, D.E., Jr. A piston model for transmembrane signaling of the aspartate receptor. *Science* **285**, 1751–1754 (1999).
9. Bilwes, A.M., Park, S.Y., Quezada, C.M., Simon, M.I. & Crane, B.R. Structure and runction of CheA, the histidine kinase central to bacterial chemotaxis. in *Histidine Kinases in Signal Transduction* (eds. Inouye, M. & Dutta, R.) 48–74 (Academic Press, San Diego, 2003).
10. Bilwes, A.M., Alex, L.A., Crane, B.R. & Simon, M.I. Structure of CheA, a signal-transducing histidine kinase. *Cell* **96**, 131–141 (1999).
11. Griswold, I.J. *et al.* The solution structure and interactions of CheW from *Thermotoga maritima*. *Nat. Struct. Biol.* **9**, 121–125 (2002).
12. Stewart, R.C., Jahreis, K. & Parkinson, J.S. Rapid phosphotransfer to CheY from a CheA protein lacking the CheY-binding domain. *Biochemistry* **39**, 13157–13165 (2000).
13. Quezada, C.M. *et al.* Structural and chemical requirements for histidine phosphorylation by the chemotaxis kinase CheA. *J. Biol. Chem.* **280**, 30581–30585 (2005).
14. Lybarger, S.R. & Maddock, J.R. Polarity in action: asymmetric protein localization in bacteria. *J. Bacteriol.* **183**, 3261–3267 (2001).
15. Gestwicki, J.E. & Kiessling, L.L. Inter-receptor communication through arrays of bacterial chemoreceptors. *Nature* **415**, 81–84 (2002).
16. Lamanna, A.C., Ordal, G.W. & Kiessling, L.L. Large increases in attractant concentration disrupt the polar localization of bacterial chemoreceptors. *Mol. Microbiol.* **57**, 774–785 (2005).
17. Studdert, C.A. & Parkinson, J.S. Crosslinking snapshots of bacterial chemoreceptor squads. *Proc. Natl. Acad. Sci. USA* **101**, 2117–2122 (2004).
18. Ames, P., Studdert, C.A., Reiser, R.H. & Parkinson, J.S. Collaborative signaling by mixed chemoreceptor teams in *Escherichia coli*. *Proc. Natl Acad. Sci. USA* **99**, 7060–7065 (2002).
19. Li, M. & Hazelbauer, G.L. Adaptational assistance in clusters of bacterial chemoreceptors. *Mol. Microbiol.* **56**, 1617–1626 (2005).
20. Kim, K.K., Yokota, H. & Kim, S.H. Four-helical-bundle structure of the cytoplasmic domain of a serine chemotaxis receptor. *Nature* **400**, 787–792 (1999).
21. Kim, S.H., Wang, W. & Kim, K.K. Dynamic and clustering model of bacterial chemotaxis receptors: structural basis for signaling and high sensitivity. *Proc. Natl. Acad. Sci. USA* **99**, 11611–11615 (2002).
22. Coleman, M.D., Bass, R.B., Mehan, R.S. & Falke, J.J. Conserved glycine residues in the cytoplasmic domain of the aspartate receptor play essential roles in kinase coupling and on-off switching. *Biochemistry* **44**, 7687–7695 (2005).
23. Starrett, D.J. & Falke, J.J. Adaptation mechanism of the aspartate receptor: electrostatics of the adaptation subdomain play a key role in modulating kinase activity. *Biochemistry* **44**, 1550–1560 (2005).
24. Boukhvalova, M., Dahlquist, F.W. & Stewart, R.C. CheW binding interactions with CheA and Tar—importance for chemotaxis signaling in *Escherichia coli*. *J. Biol. Chem.* **277**, 22251–22259 (2002).
25. Bourret, R.B., Davagnino, J. & Simon, M.I. The carboxy-terminal portion of the CheA kinase mediates regulation of autophosphorylation by transducer and CheW. *J. Bacteriol.* **175**, 2097–2101 (1993).
26. Zhao, J. & Parkinson, J.S. Mutational analysis of the chemoreceptor-coupling domain of the *E. coli* chemotaxis signaling kinase CheA. *J. Bacteriol.* (in the press).
27. Hamel, D.J. & Dahlquist, F.W. The contact interface of a 120 kD CheA-CheW complex by methyl TROSY interaction spectroscopy. *J. Am. Chem. Soc.* **127**, 9676–9677 (2005).
28. Park, S.Y., Quezada, C.M., Bilwes, A.M. & Crane, B.R. Subunit exchange by CheA histidine kinases from the mesophile *Escherichia coli* and the thermophile *Thermotoga maritima*. *Biochemistry* **43**, 2228–2240 (2004).
29. Liu, J.D. & Parkinson, J.S. Genetic evidence for interaction between the CheW and Tsr proteins during chemoreceptor signaling by *Escherichia coli*. *J. Bacteriol.* **173**, 4941–4951 (1991).
30. Zhou, J. & Parkinson, J.S. Cysteine-scanning analysis of the chemoreceptor-coupling domain of the *E. coli* chemotaxis signaling kinase CheA. *J. Bacteriol.* (in the press).
31. Boukhvalova, M., VanBruggen, R. & Stewart, R.C. CheA kinase and chemoreceptor interactions on CheW. *J. Biol. Chem.* **277**, 23596–23603 (2002).
32. Gegner, J.A., Graham, D.R., Roth, A.F. & Dahlquist, F.W. Assembly of an MCP receptor, CheW, and kinase CheA complex in the bacterial chemotaxis signal transduction pathway. *Cell* **70**, 975–982 (1992).
33. Levit, M.N. & Stock, J.B. Receptor methylation controls the magnitude of stimulus-response coupling in bacterial chemotaxis. *J. Biol. Chem.* **277**, 36760–36765 (2002).
34. Li, M. & Hazelbauer, G.L. Cellular stoichiometry of the components of the chemotaxis signaling complex. *J. Bacteriol.* **186**, 3687–3694 (2004).
35. Li, G. & Weis, R.M. Covalent modification regulates ligand binding to receptor complexes in the chemosensory system of *Escherichia coli*. *Cell* **100**, 357–365 (2000).
36. Bornhorst, J.A. & Falke, J.J. Attractant regulation of the aspartate receptor-kinase complex: limited cooperative interactions between receptors and effects of the receptor modification state. *Biochemistry* **39**, 9486–9493 (2000).
37. Liu, Y., Levit, M., Lurz, R., Surette, M.G. & Stock, J.B. Receptor-mediated protein kinase activation and the mechanism of transmembrane signaling in bacterial chemotaxis. *EMBO J.* **16**, 7231–7240 (1997).
38. Francis, N.R., Wolanin, P.M., Stock, J.B., Derosier, D.J. & Thomas, D.R. Three-dimensional structure and organization of a receptor/signaling complex. *Proc. Natl. Acad. Sci. USA* **101**, 17480–17485 (2004).
39. Shimizu, T.S. *et al.* Molecular model of a lattice of signalling proteins involved in bacterial chemotaxis. *Nat. Cell Biol.* **2**, 792–796 (2000).
40. Rao, C.V., Frenklach, M. & Arkin, A.P. An allosteric model for transmembrane signaling in bacterial chemotaxis. *J. Mol. Biol.* **343**, 291–303 (2004).
41. Studdert, C.A. & Parkinson, J.S. Insights into the organization and dynamics of bacterial chemoreceptor clusters through *in vivo* crosslinking studies. *Proc. Natl. Acad. Sci. USA* **102**, 15623–15628 (2005).
42. Levit, M.N., Liu, Y. & Stock, J.B. Mechanism of CheA protein kinase activation in receptor signaling complexes. *Biochemistry* **38**, 6651–6658 (1999).
43. Otwinowski, A. & Minor, W. Processing of X-ray diffraction data in oscillation mode. *Methods Enzymol.* **276**, 307–325 (1997).
44. Brunger, A.T. *et al.* Crystallography and NMR system: a new software suite for macromolecular structure determination. *Acta Crystallogr. D Biol. Crystallogr.* **54**, 905–921 (1998).
45. Borbat, P.P. & Freed, J.H. Multiple-quantum ESR and distance measurements. *Chem. Phys. Lett.* **313**, 145–154 (1999).
46. Borbat, P.P. & Freed, J.H. in *Biological Magnetic Resonance* Vol. 21 (eds. Berliner, L.J., Eaton, G.R. & Eaton, S.S.) 383–459 (Kluwer Academic/Plenum Publishers, New York, USA, 2001).
47. Borbat, P.P., Mchaourab, H.S. & Freed, J.H. Protein structure determination using long-distance constraints from double-quantum coherence ESR: study of T4 lysozyme. *J. Am. Chem. Soc.* **124**, 5304–5314 (2002).
48. Milov, A.D., Maryasov, A.G. & Tsvetkov, Y.D. Pulsed electron double resonance (PELDOR) and its applications in free-radicals research. *Appl. Magn. Reson.* **15**, 107–143 (1998).
49. Pfannebecker, V. *et al.* Determination of end-to-end distances in oligomers by pulsed EPR. *J. Phys. Chem.* **100**, 13428–13432 (1996).
50. Borbat, P.P., Crepeau, R.H. & Freed, J.H. Multifrequency two-dimensional Fourier transform ESR: an X/Ku-band spectrometer. *J. Magn. Reson.* **127**, 155–167 (1997).
51. Pake, G.E. Nuclear resonance absorption in hydrated crystale—fine structure of the proton line. *J. Chem. Phys.* **16**, 327–336 (1948).
52. Chiang, Y.W., Borbat, P.P. & Freed, J.H. The determination of pair distance distributions by pulsed ESR using Tikhonov regularization. *J. Magn. Reson.* **172**, 279–295 (2005).
53. Glaser, F. *et al.* ConSurf: identification of functional regions in proteins by surface-mapping of phylogenetic information. *Bioinformatics* **19**, 163–164 (2003).